HIGHER-ORDER CONCEPTUAL MODEL FOR LABYRINTH SEAL FLUTTER

Roque Corral *
Advanced Engineering Direction
Industria de Turbopropulsores S.A.U.
28108 Madrid, Spain
e-mail: roque.corral@itpaero.com

Michele Greco †
School of Aeronautics and Space
Universidad Politécnica de Madrid
28040 Madrid, Spain
e-mail: michele.greco@upm.es

Almudena Vega
School of Aeronautics and Space
Universidad Politécnica de Madrid
28040 Madrid, Spain
e-mail: almudena.vega@upm.es ‡

ABSTRACT

A simple non-dimensional model to describe the flutter onset of two-fin straight labyrinth seals [1] is extended to account for non-isentropic flow perturbations. The isentropic relationship is replaced by the more general integral energy equation of the inter-fin cavity. A new expression for the Corral & Vega stability criterion is derived which is very consistent with the previous model in the whole design space of the seal but for torsion centers located in the high-pressure side close to the seal. The new model formally depends on more dimensionless parameters since the existing parameter grouping of the previous model does not hold anymore, but this dependency is weak in relative terms. The model blends the limit where the discharge time of the inter-fin cavity is much longer than the vibration period, and the flow is nearly isentropic, and the opposite limit, where the perturbations are isothermic, gracefully. A few numerical examples obtained using a three-dimensional linearized frequency domain solver are included to support the model and show that the trends are correct but the body of the numerical work will be presented in a separated article. The matching between the work-per-cycle obtained with the model and frequency domain solver is good. It is shown that some weird trends obtained using linearized unsteady simulations are qualitatively consistent with the current model but not with the previous one [1]. The largest differences between the new and the previous model are seen when the seal is supported at the high-pressure side.

INTRODUCTION

Labyrinth seals are the oldest solution in gas turbines to limit the flow leakage between the cavities formed between the rotating and non-rotating components of compressors, combustors and turbines. Essentially, labyrinth seals are used to separate low-pressure from high-pressure regions[2]. Seals are formed by non-contacting rotating and stationary parts. The former is comprise of radial fins, resulting in series of cavities in between. The flow is successively throttled and expanded at every fin tip. The kinetic energy of the resulting wall-jet is dissipated in the inter-fin region, which in first approximation behaves as a settling chamber. The flow through the seal device is hereby reduced by repeatedly throttling the flow across the fins. Their advantage is the resistance to high-temperature flow, pressure difference and wearing.

Aeromechanic instabilities (Flutter) in labyrinth seal are known to severely impact the dynamic behavior of turbines, fans and compressors, and it is a very active field of research [3, 4, 5, 6]. The unsteady pressures in labyrinth seals can potentially cause severe aeroelastic instabilities [7, 8, 9]. A few studies on this subject were conducted in the 60's and 70's, but until recently, the understanding of labyrinth seals has been mostly based on the conclusions drawn in these pioneering works. Recently, a simple physics based conceptual model has been derived to increase the understanding of straight seal instabilities [1, 10] and new light to the problem has been shed. This model showed the existence of new dimensionless parameters which played a key role in seal instability. More recently, the model was extended to deal with stepped seals [11, 12] and new experiments conducted [13]. A short review of the relevant studies conducted on seal instabilities, as well as of their respective conclusions and shortcomings, is given next.

*Also associate professor at the Department of Fluid Dynamics and Aerospace Propulsion of the School of Aeronautics and Space, Universidad Politecnica Madrid

†Corresponding Author

‡Also senior specialist, Technology and Knowledge Division, SIEMENS-Gamesa

Alford [14] found that the support side of the seal was a key factor for the seal stability and that the tangential component of the air velocity in the inter-fin cavity had a major effect on resonances with longitudinal waves [15]. His model had some flaws since it was based on static aeroelasticity concepts but calibrated with experimental data proved to be useful. Ehrich [16] derived a simple stability parameter encompassing the effect of the torsion center location, the geometry of the cavity, and the seal fin clearance. The model was based on first principles but he did not consider the circumferential flow since his model was only valid for the zero nodal diameter case which is certainly not the most interesting one. Lewis et al. [9] experimentally described the high sensitivity of seal stability to the running clearance and later Abbot [17] identified the importance of the seal support side in combination with the ratio of the seal vibration frequency to the acoustic frequency giving rise to the widespread Abbot's criterion.

All previous studies relied on experimental data and simplified analytical models since CFD methods were not affordable at that time. Recently, there has been a renewed interest in seal flutter, and the identification of its relevant parameters using CFD tools [18, 19, 20, 13]. Despite these efforts, no new clear conclusions were drawn apart from the success in matching the scarce experimental results.

Else-ways, the classical engineering approach of using simplified models to understand the conceptual problem [4, 21, 22] and then verify the model using numerical experiments [23, 24] has again gained attention during the last years for understanding classical flutter problems. The success of these analytical models comes from their simplicity and the number of "empirical" well-known seal stability trends which are able to predict in a simple and traceable way, which is essential to assess complex engineering decisions. This is particularly true in the case of rotating seals due to their increasing role in modern high by-pass aero-engines [2], which can incorporate over 50 labyrinth seals.

Corral and Vega [1, 10] have recently proposed a new comprehensive conceptual model for seal flutter derived from first principles. The model not only conciliates the observations of Ehrich [16] and Abbot [17], but provides a more refined but still simple stability limit. A second advantage of the earlier CV model is that it delivers an estimate of the work-per-cycle and identifies new dimensionless parameters which determine the severity of the instability and the damping of the seal. This model has recently been updated to account for stepped seals and has been applied as well to estimate the damping contribution of the tip-shroud on shrouded rotor blades [11, 12]. The main limitation of the CV model is that it assumes that the flow perturbations are isentropic without further justification.

This paper presents an extension of the existing conceptual model for labyrinth seal flutter removing the hypothesis that the flow perturbations are isentropic. First, the governing equations of the seal are generalized for the non-isentropic case. Then a new expression for the work-per-cycle as a function of the dimensionless parameter is derived. Finally, some conclusions are drawn and comparisons with a few numerical simulations are presented.

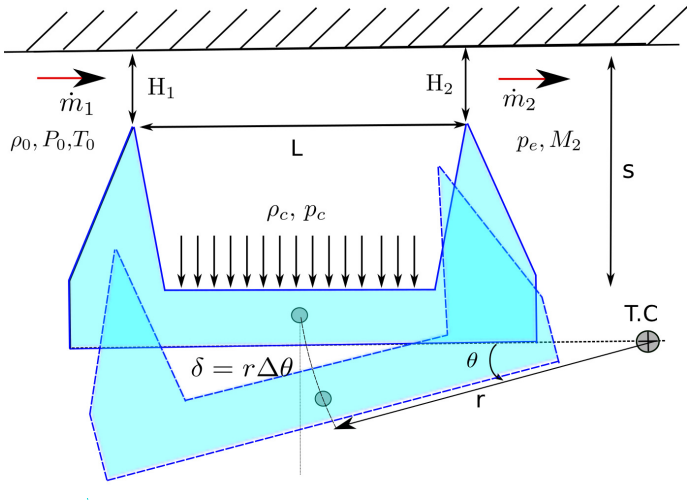

FIGURE 1. SKETCH OF AN IDEALIZED STRAIGHT SEAL CAVITY ROTATING ABOUT A TORSION CENTER LOCATED IN THE LOW PRESSURE SIDE.

GOVERNING EQUATIONS

Introduction

The original CV seal stability model and its extensions to account for stepped seals [1, 11, 12] were based in three equations, namely an ODE for the integral form of the mass conservation in the inter-fin cavity, a PDE for the momentum equation in the azimuthal direction, and the entropy conservation of the perturbed flow, which is an algebraic equation. In this work, unlike in [1, 12], the entropy conservation relationship is replaced by the integral energy equation of the inter-fin cavity. The integral energy equation is more general than the entropy equation since it does not involve any additional hypothesis about the flow, however it leads to a more complex model.

Two Dimensional Model

The semi-integral form of the mass and energy conservation equations for the volume, V_c, of the inter-fin cavity of a labyrinth seal (see Fig. 1) are formally derived in Appendix B and can be expressed as:

$$\frac{\partial}{\partial t}(\rho_c V_{c,2D}) = \dot{m}_1 - \dot{m}_2 - \frac{\partial}{\partial z}(\rho_c v_\theta V_{c,2D}) \qquad (1)$$

$$\frac{1}{\gamma-1}\frac{\partial}{\partial t}(p_c V_{c,2D}) = \dot{m}_1 H_1 - \dot{m}_2 H_2 - p_c\frac{\partial V_{c,2D}}{\partial t} - \frac{\partial}{\partial z}(\rho_c v_\theta H_c V_{c,2D}) \quad (2)$$

where ρ_c, E_c and H_c are the spatially averaged fluid density, total internal energy and total enthalpy in the cavity respectively, v_θ the circumferential velocity, $V_{c,2D}$ is the volume per unitary span of the inter-fin cavity, and $\dot{m}_1$ and $\dot{m}_2$ represent the inlet and outlet mass flows, respectively. It can also be noticed that azimuthal variations of the velocity induced by cyclic symmetric mode-shapes have been retained.

For an ideal gas, the non-dimensional quasi-steady mass flow, $\tilde{m}$, through a section of effective area, A_i, can be expressed as a function of the ratio of the inlet total pressure, P_0, and the exit static pressure, p_i, $\pi_i = P_0/p_i$, as:

$$\tilde{m} = \frac{\dot{m}\sqrt{R_g T_0}}{P_0 A_i} = \pi_i^{-\frac{\gamma+1}{2\gamma}}\sqrt{\frac{2\gamma}{\gamma-1}\left(\pi_i^{\frac{\gamma-1}{\gamma}}-1\right)} = f(\pi_i,\gamma) \quad (3)$$

where T_0 is the total temperature. The flow through the knife-seal is assumed quasi-stationary since the characteristic length of the inlet and outlet gap of the inter-fin seal cavity, H_1 and H_2 respectively, are much smaller than the characteristic size of the inter-fin cavity, L, and therefore the through-flow time through the fin is much smaller than the cavity discharge time. Moreover, it is assumed that:

1. The process is adiabatic ($RePr \gg 1$), and the work added by the seal rotation is negligible and therefore the mean total temperature in the inter-fin cavity is constant and equal to that of the inlet.
2. The work associated to the viscous forces and the wall heat flux in the seal are negligible.

Under these hypotheses the continuity equation (Eq. 1) reduces to:

$$\frac{\partial}{\partial t}(\rho_c V_{c,2D}) + \frac{\partial}{\partial z}(\rho_c v_\theta V_{c,2D}) = \frac{P_0 A_1}{\sqrt{R_g T_0}} f(P_0/p_c,\gamma) - \frac{p_c A_2}{\sqrt{R_g T_0}} f_e \quad (4)$$

where p_c is the static pressure at the cavity, $\pi_s = P_0/p_c$ is the cavity pressure ratio and f_e is defined as:

$$f_e = \sqrt{\gamma}\left(\frac{\gamma+1}{2}\right)^{-\frac{\gamma+1}{2(\gamma-1)}}. \quad (5)$$

The generalization of the continuity equation for an unchoked exit can be found in the Appendix A of reference [1].

The momentum equation in the circumferential direction is:

$$\frac{\partial v_\theta}{\partial t} + v_\theta\frac{\partial v_\theta}{\partial z} + \frac{1}{\rho_c}\frac{\partial p_c}{\partial z} = 0 \quad (6)$$

In the original CV model [1] the mass and momentum equations of the inter-fin cavity, together with the barotropic relationship, given in this case by the isentropic condition (which yields a relationship between the density and pressure in the cavity, $\rho_c = \rho_c(p_c)$), formed a system of an Ordinary Differential Equation (ODE) and a Partial Differential Equation (PDE) to determine $p_c(t)$ and $v_\theta(t)$. The time variation of the problem was due to the temporal changes of $V_{c,2D}(t)$, $A_1(t)$ and $A_2(t)$, which are known. However, in this case a new barotropic condition need to be sought.

Steady State

The steady solution in the model is obtained by imposing that $\dot{m}_{1,s} = \dot{m}_{2,s}$, $H_{1,s} = H_{2,s}$ and $\partial/\partial z = 0$. It will be assumed for the sake of simplicity that $A_1 = A_2 = Hd$, where H is the mean clearance between the fin seal and the stationary part of the inlet and outlet of the seal cavity, and d is an unitary distance in the tangential direction, z. Alternatively, the mean variables in the seal can be obtained from a higher-order model such as the solution of a Computational Fluid Dynamics (CFD) model. This is actually the approach that will be followed in this work since the steady flow modelization associated to the CV model is very simple. For more details see [1].

Barotropic Relationship

The derivation of this higher order model is really more involved than the original CV model [1], because of the inclusion of the energy equation. This is particularly true if a systematic linearization of the governing equations is performed and subsequently traveling-wave solutions of the problem are sought. This procedure is not only tedious but would not shed much light on the physics of the problem. Alternatively, a new relationship to replace the isentropic condition for the perturbations ($p_c' = \rho_c' a_0^2$) has been seeked. It will be shown that it is possible to find a relation of the form $\rho_c' = \rho_c'(p_c', \omega)$, where ω is the vibration angular frequency of the seal.

If the vibration amplitude of the seal is small enough, the flow and geometric variables can be decomposed into two parts: a mean background flow, and a small and periodic unsteady perturbation. In this case the density, static pressure, the volume of the cavity and the seal gap areas can be written as:

$$\begin{aligned} \rho_c &= \rho_{c,s} + \rho_c'(t),\ p_c = p_{c,s} + p_c'(t), \\ V_c &= V_{c,s} + v_c(t),\ A_j = A_{j,s} + a_j(t). \end{aligned} \quad (7)$$

It is convenient to define also the more compact mass-flow and total enthalpy variables:

$$\dot{m}_{1,2} = \dot{m}_s + \Delta\dot{m}_{1,2} \text{ and } H_c = H_{c,s} + H_c'. \quad (8)$$

The linearization of the r.h.s. of the system of Eqs. 1 and 2 yields:

$$\begin{aligned} \frac{d(\rho_c V_c)}{dt} &= (\Delta\dot{m}_1 - \Delta\dot{m}_2) - \frac{\partial(\rho_c v_\theta V_{c,2D})}{\partial z} \\ \frac{1}{\gamma-1}\frac{d(p_c V_c)}{dt} &= (\Delta\dot{m}_1 - \Delta\dot{m}_2)H_{c,s} - \frac{\partial(\rho_c v_\theta H_c V_{c,2D})}{\partial z} \\ &\quad - p_{c,s}\frac{\partial v_c}{\partial t} - \dot{m}_s H_c' \end{aligned} \tag{9}$$

subtracting from the semi-linearized energy equation the continuity equation multiplied by $H_{c,s}$, it is readily obtained that:

$$\begin{aligned} \frac{d}{dt}\left[\left(\frac{p_c}{\gamma-1} - \rho_c H_{c,s}\right)V_c\right] = & -\dot{m}_s H_c' - p_{c,s}\frac{\partial v_c}{\partial t} \\ & -\frac{\partial}{\partial z}\left(\rho_c v_\theta H_c' V_{c,2D}\right). \end{aligned} \tag{10}$$

where the perturbed total enthalpy is:

$$H_c' = H_{c,s}\left(\frac{p_c'}{p_{c,s}} - \frac{\rho_c'}{\rho_{c,s}}\right). \tag{11}$$

The third term of the r.h.s. of Eq. 10 is a second order term which can be neglected if it is assumed that the mean value of the flow circumferential velocity in the inter-fin cavity, $v_{\theta,s}$, is zero because the flow is described in the relative frame of reference of the fluid. In this case Eq. 10 finally becomes:

$$\frac{d}{dt}\left[\left(\frac{p_c}{\gamma-1} - \rho_c H_{c,s}\right)V\right] = -\dot{m}_s H_{c,s}\left(\frac{p_c'}{p_{c,s}} - \frac{\rho_c'}{\rho_{c,s}}\right) - p_{c,s}\frac{\partial v_c}{\partial t}. \tag{12}$$

This expression can be non-dimensionalised to obtain the following dimensionless linearized combination of the mass and energy equations:

$$\Omega\left[\frac{\partial\tilde{p}}{\partial\tau} - \gamma\frac{\partial\tilde{\rho}}{\partial\tau}\right] = -(\tilde{p} - \tilde{\rho}) \tag{13}$$

The only dimensionless parameter present in Eq. 13 is the non-dimensional discharge time of the inter-fin cavity:,

$$\Omega = \omega\frac{p_{c,s}V_{c,s}}{\dot{m}_s a_c^2}. \tag{14}$$

Though Eq. 13 has no spatial derivatives, solutions are sought in traveling-wave form to deal later on with more generic expressions containing spatial derivatives.

$$\begin{aligned} \tilde{p} &= \tilde{p}_s\sin(\tau+\tilde{z}) + \tilde{p}_c\cos(\tau+\tilde{z}) \\ \tilde{\rho} &= \tilde{\rho}_s\sin(\tau+\tilde{z}) + \tilde{\rho}_c\cos(\tau+\tilde{z}) \end{aligned} \tag{15}$$

It is not difficult to foresee that by injecting expression 15 into Eq. 13 it is possible to find out expressions of the form:

$$\tilde{\rho}_s = \tilde{\rho}_s(\tilde{p}_s, \tilde{p}_c, \Omega, \gamma) \text{ and } \tilde{\rho}_c = \tilde{\rho}_c(\tilde{p}_s, \tilde{p}_c, \Omega, \gamma). \tag{16}$$

which play the role of a barotropic relationship for the perturbations.

Several conclusions can be drawn by inspecting Eq. 13. If the seal vibration is slow enough, (i.e. $\Omega \ll 1$) the barotropic relationship reduces to $\tilde{p} = \tilde{\rho}$. In other words, the flow perturbations are isothermic. This was the hypothesis used by Ehrich [16] to derive his 0th nodal diameter model for the stability of a generic inter-fin cavity. On the contrary, if the seal vibration is fast and $\Omega \gg 1$ then $\tilde{p} = \gamma\tilde{\rho}$, which essentially states that the perturbations are isentropic.

Linearized Model

In this subsection a blend of the new barotropic condition with the formulation of the previously published models [1, 12] is performed. The first step is to write the linearized continuity equation without making use of the isentropic condition ($p_c' = \rho_c' a_c^2$) to remove the dependence on the density in the equation, which is contrary to the original CV model. In this case the linearized mass conservation equations is:

$$\begin{aligned} \frac{1}{\dot{m}_s}\left[V_{c,s}\frac{\partial\rho_c'}{\partial t} + \rho_{c,s}\frac{\partial v_c}{\partial t} + \rho_{c,s}V_{c,s}\frac{\partial v_\theta}{\partial z}\right] = & -h'(\pi_s)\frac{p'_c}{p_{c,s}} \\ & + \frac{a_1}{A_{1,s}} - \frac{a_2}{A_{2,s}} \end{aligned} \tag{17}$$

where a_c is the sound speed in the inter-fin cavity and $h'(\pi_s)$ is a known expression of π_s (see appendix A of reference [1] for further details). The h' function monotonically decreases with the total pressure ratio of the seal, π_T, which is actually very steep for low pressure ratios. It reaches an asymptotic value of about 2,6 when the seal is choked.

The following dimensionless linearized mass conservation equation:

$$\Omega\left[\gamma\frac{\partial\tilde{\rho}}{\partial\tau} + \gamma\frac{\partial\tilde{v}_c}{\partial\tau} + \frac{1}{St}\frac{\partial\tilde{v}_\theta'}{\partial\tilde{z}}\right] = -h'\tilde{p} + \tilde{a}_1 - \tilde{a}_2 \tag{18}$$

is obtained by using the previously defined dimensionless variables together with:

$$\tilde{v}_\theta' = \frac{\gamma v_\theta}{a_c}, \tilde{z} = \frac{zND}{R} \tag{19}$$

where R is the radius of the seal, a_c the speed of sound in the inter-fin cavity, and ND the mode-shape nodal diameter. The only non-dimensional parameters present again in Eq. 18 are Ω and, St, the ratio of the vibration to the acoustic frequency

$$St = \frac{\omega L_\theta}{a_c} = \frac{\omega}{\omega_{ac}}. \tag{20}$$

Analogously, and assuming that the mean circumferential velocity is null, i.e. there is no swirl velocity or the equations are written in the relative frame of reference, the following dimensionless form of the circumferential momentum equation is obtained:

$$St\frac{\partial\tilde{v}_\theta'}{\partial\tau} + \frac{\partial\tilde{p}}{\partial\tilde{z}} = 0. \tag{21}$$

The equations 18 and 21 together with expression 13 form a system of two PDEs and one ODE which has to be solved with the proper initial and boundary conditions.

Geometry Variations

The solution of the problem requires the specification of the temporal and spatial variations of the seal volume, $V_{c,2D}(t,z)$, and the gaps $A_{1,2}(t,z)$. The solution of Eqs. 18 and 21 was obtained for the particular case of a straight seal whose motion can be approximated as a rotation about a torsion center, TC, aligned with the center of the seal and located at a certain distance, r, from it [1] (see Fig. 1). For a straight seal the time variations of the control volume and the inlet and outlet areas can be expressed, in non-dimensional form, as:

$$\begin{aligned} \tilde{a}_{1,2} &= \frac{(r \pm L/2)}{H_{1,2}}\theta \\ \tilde{v}_c &= \frac{r}{s}\theta \end{aligned} \tag{22}$$

where L is the fin spacing, and s the inter-fin cavity height. Assuming for simplicity that the mean clearance is the same for both, inlet and outlet teeth, $H_1 = H_2 = H$, and that the motion of the seal is harmonic and can be written in traveling wave form:

$$\theta = \Delta\theta \sin\eta \tag{23}$$

where $\eta = \tau + \tilde{z}$, is the non-dimensional coordinate in the traveling waves frame of reference, then Eq. 18 yields:

$$\tilde{\Omega}\left[\gamma\frac{d\hat{\rho}}{d\tau} + \tilde{e}h'\cos\eta + \frac{1}{St}\frac{\partial\hat{v}'_\theta}{\partial\tilde{z}}\right] = -\hat{p} + \sin\eta. \tag{24}$$

If the unsteady pressure and the azimuthal velocity are renormalized as:

$$\hat{p} = \frac{1}{\varepsilon}\tilde{p},\ \hat{\rho} = \frac{1}{\varepsilon}\tilde{\rho}\ \hat{v}'_\theta = \frac{1}{\varepsilon}\tilde{v}'_\theta \text{ with } \varepsilon = \frac{L\Delta\theta}{Hh'}. \tag{25}$$

If $\varepsilon \ll 1$, the unsteady pressure perturbations are small compared to the mean pressure of the cavity, $p_{c,s}$, and therefore Eq. 24 is an accurate representation of the solution. The parameter $\tilde{e}$ can be regarded either as the non-dimensional seal clearance, or the non-dimensional distance between the torsion center and the cavity midpoint, and essentially is a geometric parameter. It should be recalled [1] that

1. The characteristic amplitude of the unsteady pressure in the seal cavity, is $p'_c \sim \varepsilon\ p_{c,s}$ if $\tilde{\Omega} \sim 0(1)$.
2. Seals with tight clearances, H, can generate large unsteady pressures,
3. Unsteady pressure scales linearly with the amplitude of the vibration, $\Delta\theta$.

The main advantage of this form is that it reduces the number of non-dimensional parameters to four. In this case

$$\hat{p} = \hat{p}(St, \Omega, \tilde{e}, h') \tag{26}$$

The main difference with the CV model is that in this case the dependence with h' cannot be grouped with the other three parameters because of the more generic barotropic relationship.

SOLUTION OF THE SEAL STABILITY MODEL

The final step is to seek for periodic solutions, both in time and space, of the non-dimensional continuity and momentum equations (Eqs. 18 and 21, respectively) together with the barotropic relationship (Eq. 13). Expressing the non-dimensional unsteady pressure, density and circumferential velocity as:

$$\begin{aligned} \hat{p} &= \hat{p}_s\sin(\tau+\tilde{z}) + \hat{p}_c\cos(\tau+\tilde{z}) \\ \hat{\rho} &= \hat{\rho}_s\sin(\tau+\tilde{z}) + \hat{\rho}_c\cos(\tau+\tilde{z}) \\ \hat{v}'_\theta &= \hat{v}_s\sin(\tau+\tilde{z}) + \hat{v}_c\cos(\tau+\tilde{z}) \end{aligned} \tag{27}$$

and injecting the above expressions in Eq. 21, it is readily obtained that:

$$\hat{v}_s = -\hat{p}_s/St \text{ and } \hat{v}_c = -\hat{p}_c/St. \tag{28}$$

This relationship is used to remove the unknown velocity from Eqs. 24 and 13, and to obtain, after a considerable amount of algebra, the following solution for the out-of-phase component of the unsteady pressure:

$$\hat{p}_c = -\bar{\Omega}\left[\left(\tilde{e}h'_{eff} + \left(1 - \frac{1}{St^2}\right)\right)\right] \Big/ \left[\tilde{\mathrm{I}} + \bar{\Omega}^2\left(1 - \frac{1}{St^2}\right)^2\right] \tag{29}$$

of the general problem, where:

$$\bar{\Omega} = \hat{\Omega}\tilde{\Omega}, \text{ with } \quad \hat{\Omega} = \gamma\frac{1+\gamma\Omega^2}{1+\gamma^2\Omega^2} \tag{30}$$

and

$$\frac{\tilde{e}h'_{eff}}{\tilde{e}h'} = \frac{1+\alpha}{\hat{\Omega}}, \quad \alpha = \gamma(\gamma-1)\frac{\tilde{\Omega}\Omega}{1+\gamma^2\Omega^2}, \quad \tilde{\mathrm{I}} = (1+\alpha)^2 \tag{31}$$

It is important to remark that a big effort has been devoted to deriving an expression which resembles the simple expression obtained in [1]. Actually, the functional form of the out-of-phase component of the unsteady pressure (Eq. 29) is identical to that obtained in [1] if the following identities are fulfilled $\bar{\Omega} \equiv \tilde{\Omega}$, $\tilde{e}h'_{eff} \equiv \tilde{e}h'$ and $\tilde{\mathrm{I}} \equiv 1$.

A surprising result is that the isentropic limit is never recovered even in the high-frequency limit when $\Omega \gg 1$. Figure 2 displays $\hat{\Omega}$ as a function of the non-dimensional frequency, Ω. It can be seen that $\hat{\Omega}$ varies smoothly between $\hat{\Omega}(0) = \gamma$ and $\hat{\Omega}(\Omega \to \infty) \to 1$. The function $\hat{\Omega}$ tends very quickly to one since for $\Omega \gg 1$, $\hat{\Omega} \simeq 1 + \Omega^{-2}(\gamma-1)/\gamma^2$. This means for instance that for most of the realistic cases $\bar{\Omega} \simeq \tilde{\Omega}$. This result is fully consistent with the isentropic limit. However, this is not the case for the function $\alpha = \alpha(\Omega)$ which when $\Omega \to \infty$ tends to $\alpha \to (\gamma-1)/(\gamma h')$ (see Fig. 2 for a representation of the function). The function α is always small and bracketed in the interval $\alpha \in [0, 0.11]$. For choked seals $\alpha(\Omega)$ is about $\alpha \simeq 0.11$. Same conclusions could be outlined for the function $\tilde{\mathrm{I}}$.

The ultimate reason for this is that for $\Omega \gg 1$, Eq. 13 represents an isentropic relationship for the perturbations within an error of $\mathscr{O}(\Omega^{-1})$. In this case, the dimensionless in-phase and out-of-phase unsteady pressure in the cavity are of order $\mathscr{O}(1)$ and

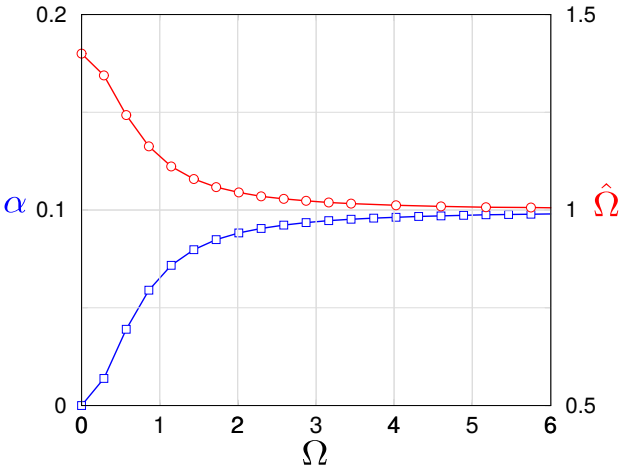

FIGURE 2. AUXILIARY FUNCTIONS AS A FUNCTION OF THE DIMENSIONLESS FREQUENCY Ω FOR A CHOKED SEAL. $\bigcirc : \hat{\Omega}$; $\square : \alpha$.

$\mathscr{O}(\Omega^{-1})$ respectively. This means that the out-of-phase component of the unsteady pressure in the cavity, which is much smaller than the in-phase one, is of the same order as the error generated assuming that the flow is isentropic. Fortunately, the function alpha is bounded by $0,11$, which is small, but this could not had been anticipated without solving the whole problem.

Work per Cycle

The work-per-cycle, W_{cyc}, created by the unsteady pressure field on a straight seal can be expressed as follows:

$$W_{cycle} = \int_0^T \int_\Sigma p_c'(t)\, \mathbf{v}.\mathbf{n}\, dA\, dt \tag{32}$$

where $\mathbf{v}$ and $\mathbf{n}$ are, respectively, the velocity and the normal direction at the seal surface. It has been assumed that the pressure within the cavity is uniform, and that the contribution of the seal fins to the W_{cyc} is negligible. It can be noticed that only the out-of-phase component of the pressure appears in the expression of the W_{cyc}. The stability criteria used in this work is such that when the work-per-cycle exerted by the fluid forces onto the seal is positive, then the fluid is amplifying the vibration and the seal is unstable, whereas if it is negative, the fluid is absorbing energy from the seal, the vibration is damped and the seal is stable.

The non-dimensional work-per-cycle is defined as:

$$\tilde{W}_{cyc} = \frac{W_{cyc}}{\pi p_{c,s} \delta^2 S L/|r| H h'} = \text{sign}(r)\hat{p}_c \tag{33}$$

where $\delta = r\Delta\theta$ is the seal torsion displacement, and $S = 2\pi RL$, is the seal surface. It is concluded that the dimensionless work-per-cycle of a two-fin sraight seal depends hence solely on the following four dimensionless parameters:

$$\tilde{W}_{cyc} = \tilde{W}_{cyc}\left(\tilde{\Omega}, St, \tilde{e}h', h'\right) \tag{34}$$

which physically accounts for the effect of the fluid steady state, the geometry of the cavity, the clearance between the fins and the steady flow-field, the torsion center location, and the vibration frequency. The effect of the Re, Pr, and Ec numbers on the steady state of the fluid has been disregarded since they are deemed to have only a second order influence on the work-per-cycle through their slight influence on the steady base flow. The effect of geometric parameters such as s/L, H/L or α, in the steady state flow of the seal are of larger importance but cannot be retained in this simple model where the mean flow is considered as given. The main difference with the original CV model [1] is that the parameters $\tilde{e}$ and h' cannot be formally grouped into a single parameter.

RESULTS

Zero Nodal Diameter Case

Model discussion Although the interest of the zero nodal diameter from an engineering point of view is limited, this case is discussed first because it is the simplest and there are some implications which can be extended for higher nodal diameter cases. The non-dimensional $\tilde{W}_{cyc}$ of the zero nodal diameter case is described next. This problem was first addressed by Ehrich [16] and recently by Corral and Vega [1]. The results of both works are consistent with the sole difference that the former assumed that the flow perturbations were iso-thermic and the latter isentropic. The dimensionless work-per-cycle can be written as:

$$\tilde{W}_{cyc} = \text{sign}(\tilde{e}h')\hat{p}_c = -(1+\tilde{e}h'_{eff})\frac{\bar{\Omega}}{(\bar{\Omega}^2+\tilde{1})} \tag{35}$$

where the out-of-phase component of the pressure corresponds to the expression 29 in the limit $St \to \infty$. This expression is very similar to that derived in [1] with the main difference that $\tilde{e}h'_{eff} = \tilde{e}h'_{eff}(\Omega)$ (see Eq. 31). The new variable $\bar{\Omega} = \bar{\Omega}(\tilde{\Omega}, \hat{\Omega})$ is just a smooth mapping of the variable $\tilde{\Omega}$. As it has been discussed before, the impact of the new barotropic condition in $\bar{\Omega}$ is small but the impact in $\tilde{e}h'_{eff}$ can be up to 10%, leading to a qualitative change in the stability limit depending on the position of the torsion center.

Figure 3 displays the $\tilde{W}_{cyc}$ as a function of the dimensionless frequency, $\tilde{\Omega}$, for a seal with a pressure ratio of $\pi_T = 2$ ($h' = 2.8$). The isentropic model derived in [1] is plotted as a reference to evaluate the variation induced by the new formulation. It can be seen that when the seal is supported at the LPS ($\tilde{e}h' > 0$) the impact of the higher-order model is very small. This is because of the variation of $\tilde{e}h'_{eff}$ with Ω is small ($\gamma^{-1} < \tilde{e}h'_{eff}/\tilde{e}h' < 1.1$) and that of $1+\tilde{e}h'$ even smaller. Unlike what was expected in the isentropic model, when the support of the seal is located in the HPS, the stability can change with the non-dimensional frequency. In Fig. 3 (b) is observed that for the lowest values of $\tilde{\Omega}$

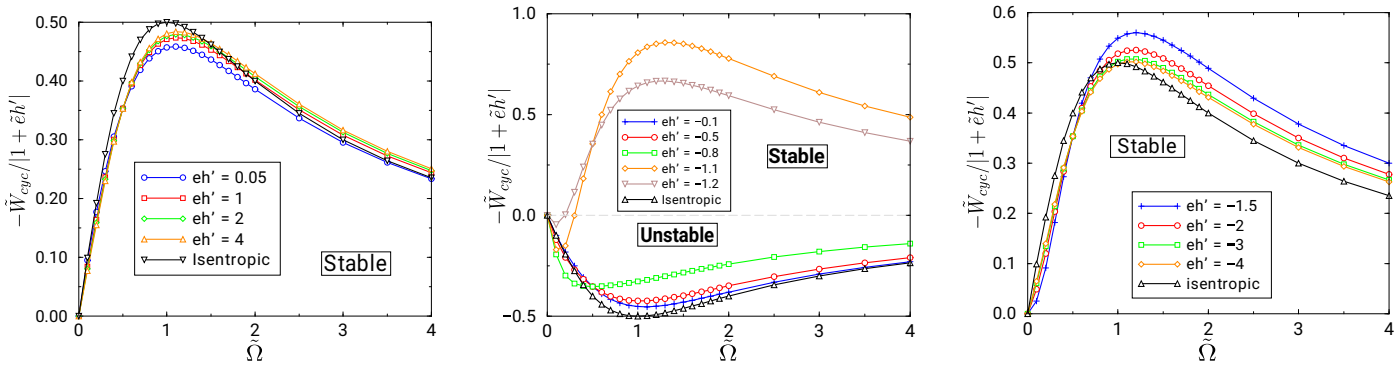

(a) Low-Pressure Side (b) High-pressure side ($-\gamma < \tilde{e}h' < 0$) (c) High-pressure side ($\tilde{e}h' < -\gamma$)

FIGURE 3. DIMENSIONLESS WORK-PER-CYCLE NORMALIZED WITH $|1+\tilde{e}h'|$ AS A FUNCTION OF THE DIMENSIONLESS VIBRATION FREQUENCY FOR THE 0TH NODAL DIAMETER. ISENTROPIC CURVE DENOTES THE EXPRESSION DERIVED IN [1].

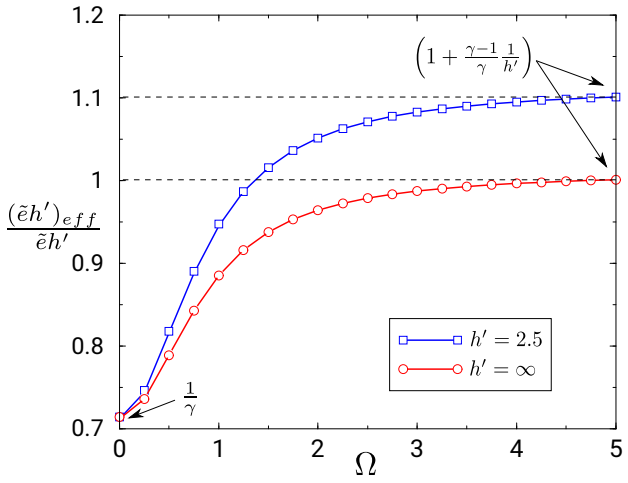

FIGURE 4. VARIATION OF THE EFFECTIVE DIMENSIONLESS GAP PARAMETER, $(\tilde{e}h')_{eff}$, AS A FUNCTION OF THE DIMENSIONLESS FREQUENCY, Ω, AND THE PRESSURE RATIO OF THE SEAL.

an unstable zone exists when $\tilde{e}h' \to -\gamma$. However, for $\tilde{e}h' < -\gamma$ the trend of the higher-order model becomes again close to that of the isentropic model (see Fig. 3 (c)). Nonetheless, seals supported in the HPS have a higher sensitivity to the torsion center position than those supported in the LPS because $1+\tilde{e}h'_{eff}$ is smaller.

Figure 4 shows the variation of $\tilde{e}h'_{eff}$ with Ω and the pressure ratio (let us recall that $h'(\pi_c)$). It can be seen that when the non-dimensional frequency is low ($\Omega \ll 1$), $\tilde{e}h'_{eff} \to \tilde{e}h'/\gamma$, on the contrary for high values of the frequency ($\Omega \gg 1$), $\tilde{e}h'_{eff} \to \tilde{e}h'(1+(\gamma-1)/(\gamma h')$. Depending on the pressure ratio of the seal, the previous asymptotic value tends to $\tilde{e}h'_{eff} \to \tilde{e}h'$ for small pressure ratios ($h' \gg 1$), or to $\tilde{e}h'_{eff} \to 1.1\,\tilde{e}h'$ approximately, for choked seals ($h' \to h'_{min} \simeq 2.6$, see [1]). All these variations of $\tilde{e}h'_{eff}$ with Ω are considered small and its effect slightly affects previous results [1].

If the torsion center is located either on the LPS or on the HPS but far away from the seal midpoint, the seal is always stable (see Figs. 3 (c) and 5). However, there is an intermediate region of torsion centers for which the stability can change when the frequency is changed. This is the third region marked in the new stability map for the 0^{th} nodal diameter (see Fig. 5). Within this region which spans between $-\gamma < \tilde{e}h' < -(1+(\gamma-1)/(\gamma h'_{min}))^{-1}$ the stability can change with the frequency (see Fig. 3 (b)). This behavior is qualitatively different from that of the original CV model and we will give some indications that this can be observed in unsteady numerical simulations.

Figure 5 (a) illustrates the former stability criterion derived in [1], which matches the Ehrich's criterion [16] if properly corrected for isentropic flows. The main idea is that the stability of the 0th ND depends on the position of the torsion center but not on the frequency. This is also the case in the new model for most of the torsion center locations. However, there is a significant region in the HPS where the stability depends on the frequency and the pressure ratio of the seal because $\tilde{e}h'_{eff}$ is a function of $\tilde{\Omega}$ (see Fig. 5 (b)). This is the new understanding and had not been detected by the previous models.

Figure 5 (b) sketches the new 0th ND stability criterion. As it has been previously mentioned, seals supported in LPS are always stable. However, in the new model the unstable region grows as the non-dimensional frequency is decreased. The critical values of $\tilde{e}h'$ in the HPS depend on the pressure ratio of the seal. When $\tilde{\Omega} \to \infty$ the critical limit curves (depicted in red) are obtained between $\tilde{e}h' = -1$, for very low-pressure ratios, and $\tilde{e}h' = -(1+(\gamma-1)/(\gamma h'_{min}))^{-1}$, for choked seals, the actual value depending on the pressure ratio. In the low-frequency regime ($\tilde{\Omega} \to 0$) the critical value tends to $\tilde{e}h' = -\gamma$, irrespectively of the seal pressure ratio.

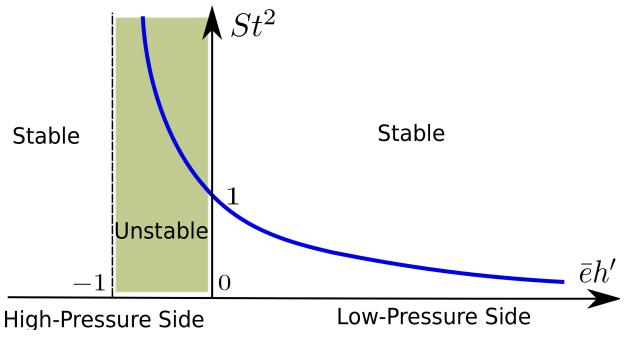

(a) Ehrich [16] and CV [1] Stability Criteria

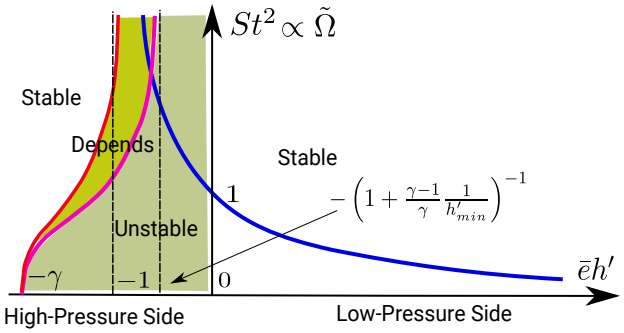

(b) New Stability criterion for $ND = 0$

FIGURE 5. STABILITY CRITERIA FOR THE ZERO NODAL DIAMETER CASE AS A FUNCTION OF THE DIMENSIONLESS TORSION CENTER ($\bar{e}h'$) AND FREQUENCY (St^2 OR $\tilde{\Omega}$) . GENERAL STABILITY CRITERIA OF THE CV MODEL (BLUE CURVE).

Preliminary CFD exploration In this sub-section, the predictions of the analytical model are compared against 3D unsteady simulations. Due to the complexity of the discussion of the comparison of the numerical results with the different conceptual models, the authors have decided to publish this work in a separate article. However, the authors want to give in this subsection a flavor of how the model compares with simulations and what is the level of accuracy that can be expected. Nonetheless, the numerical results shown here are not meant to be a thorough validation exercise.

All the simulations have been carried out with a well validated linearized Navier-Stokes solver implemented in the frequency domain named as $Mu^2s^2T - L$ [25]. The results presented here correspond to a simplified straight two-fin seal ($L/s = 1.58$, $H/s = 2 \times 10^{-2}$) with a pressure ratio of 2,0. Two large cavities located upstream and downstream of the seal are use to feed and discharge the seal (see Fig. 6 (a)). The inlet and outlet are large to ensure that high-energy jets are not created in the cavity. Special attention has been paid to avoid exciting the acoustic resonances of the upstream and downstream cavities to ease the comparison with the model. The presence of resonances in the

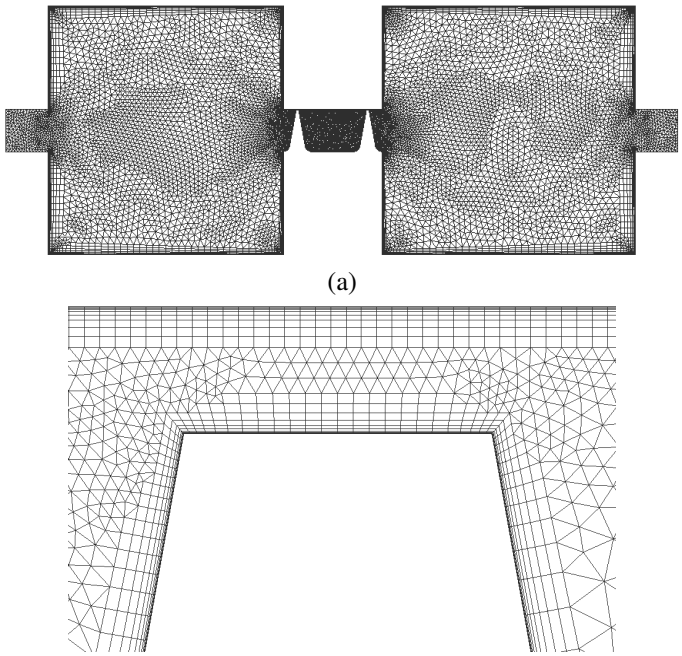

(a)

(b)

FIGURE 6. SKETCH AND MESH OF A SIMPLIFIED SEAL GEOMETRY USED TO VALIDATE THE MODEL. (A) OVERVIEW OF THE COMPUTATIONAL DOMAIN. (B) CLOSE-UP OF THE SEAL KNIFE AND GAP.

adjacent cavities can hinder the comparison with the analytical models. The computational grid consists of a 2D hybrid mesh [26] extruded in the circumferential direction in a 10° sector containing about 350,000 points. The resolution in the seal gap and the fin region is high to properly represent the wall jet created by seal knives (see Fig. 6 (a)). The standard $k-\omega$ turbulence model is used and the phase-shifted boundary conditions are applied in the lateral boundary conditions of the control volume to accomodate arbitrary circumferential wave-lengths. The seal moves as a rigid body about a prescribed torsion center and only the work exerted on the cavity land and on the seal knifes is retained.

Figure 7 compares the non-dimensional work-per-cycle, $\tilde{W}_{cyc}$, (see Eq. 35) normalized by $|1+\bar{e}h'|$ with the W_{cyc} obtained from 3D linear analyses non-dimensionalized in the same form. Aiming at improving the prediction capability of the model, the mean static pressure in the inter-fin cavity obtained from the steady-state solution of the seal has been used to non-dimensionalize the W_{cyc} instead of that delivered by the model. The effective gaps of the seal derived from the CFD have been used in the formulation instead of the nominal geometric values to enhance the accuracy of the model.

The first impression is that the degree of matching is surprisingly good, especially if it is recalled that the W_{cyc} derived from several unsteady Navier-Stokes simulations is compared against a simple

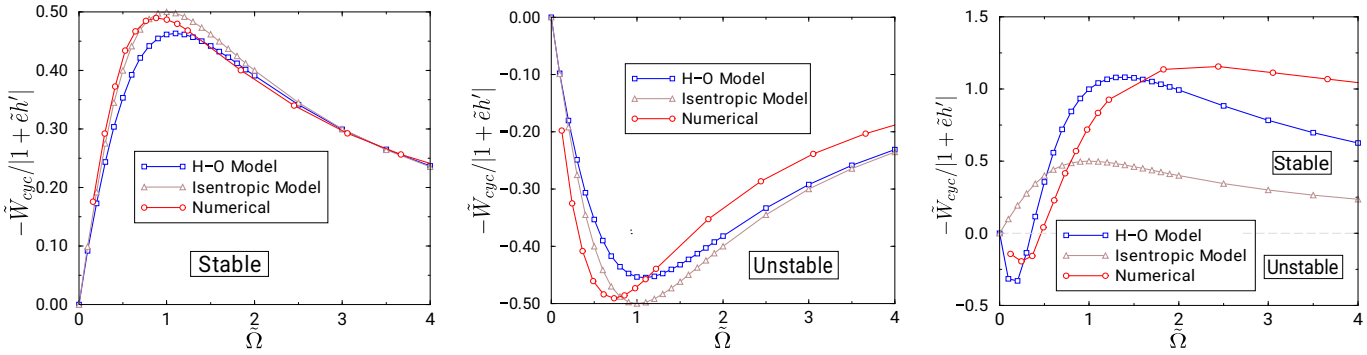

(a) LPS ($\tilde{e}h' = +0.24$) (b) HPS ($\tilde{e}h' = -0.06$) (c) HPS ($\tilde{e}h' = -1.06$)

FIGURE 7. COMPARISON OF THE HIGH ORDER AND CV MODEL WITH CFD RESULTS FOR A TWO-FIN STRAIGHT SEAL WITH A PRESSURE RATIO OF 2.0 FOR SELECTED TORSION CENTERS AND THE 0TH NODAL DIAMETER. (A): $r/L = 2$ (B):$r/L = -1$ (C): $r/L = 7$.

analytical expression. The matching when the torsion center is located on the LPS side (Fig. 7 (a)) is good for both analytical models, and the trend with the frequency is very well predicted.

It is remarkable that the conclusion derived from Eq. 13, i.e. that at low-frequency vibrations ($\Omega \ll 1$) the perturbations are isothermic, whereas at high frequency ($\Omega \gg 1$) the perturbations are isentropic, has been numerically verified in the linearized Navier-Stokes simulations performed to construct Fig. 7. This is a relevant step, since although the current model is qualitatively similar to the original CV model, some quantitative differences can be observed as will be shown next.

Figure 7 (b) shows that when the torsion center is located on the HPS the amplitude of the maximum work-per-cycle is under-predicted. It is important to stress that the analytical model assumes that the unsteady pressure is uniform in the whole inter-fin cavity. The numerical simulations confirm that this is actually the case, except in the downstream fin which is impinged by the wall jet flow created in the inlet fin. The unsteady pressure is higher in this region than in the rest of the cavity. This imbalance of unsteady pressure between both fins increases the W_{cyc} of the seal, especially when the torsion center is located in the HPS because of the displacement of the exit fin is higher than that of the inlet fin.

Finally, when the seal is vibrating about a torsion center located on the HPS far away of the seal center, the behavior is weird (see Fig. 7 (c)). This anomalous trend, which was not included in the original CV model [1], is somewhat predicted by the new model.

It is noteworthy that a value of $\tilde{e}h' = -1.06$, which is negative, is obtained with the torsion centre located in the LPS ($r/L = 7$). This is due to the effective clearance of the seal. As described in [10] the sign of the non-dimensional torsion centre can also change depending on the ratio of the effective clearance of both fins. The discharge coefficient of each gap has been extracted from the steady simulation and an effective value of $\tilde{e}$ has been used in the expressions. Particularly, according to the CFD results for this seal, $H_{2,eff} < H_{1,eff}$, and the non-dimensional torsion center changes its sign in the LPS. This issue will be addressed in future works. It is important to stress also that the physical work-per-cycle in the cases of Fig. 7(c) are about two orders of magnitude less than those of Figs. 7(a) and 7(b). This is due to the fact that when the torsion center is far away from the seal center, the difference between the displacement of the inlet and outlet fin is small, and therefore the unsteady pressure is small since it is mainly driven by the variation of the inter-fin cavity volume. Moreover, the plot is scaled with $|1+\tilde{e}h'|$ which is close to zero. In this context, even a small correction in the calculation of the effective gap can lead to misleading results.

It is concluded that both, the higher order model and the original CV model [1] are able to predict not only the stability trends of the W_{cyc} of the seal, but also quantitative results, depending on the torsion center region. It is important to highlight also that to obtain meaningful results it is important to feed the analytical model with the correct parameters. The discussion about which are the actual value of the parameters that must be entered into the model is very involved, and it is postponed for the future. However, it is important to stress that the model has not been empirically tuned to obtained the results presented in Fig. 7. The model needs to be properly informed from the steady state values, in particular the mean static pressure in the cavity and, more importantly, the effective clearance of the fin seals. This is not considered a deficiency of the model but raises the question of how to use the model.

General Case Stability Criterion

Though the 0th ND case is informative and an introductory case to understand the implications of the new model, circumferential variations need to be accounted for to obtain meaningful results. In this case, the critical reduced frequency is obtained by impos-

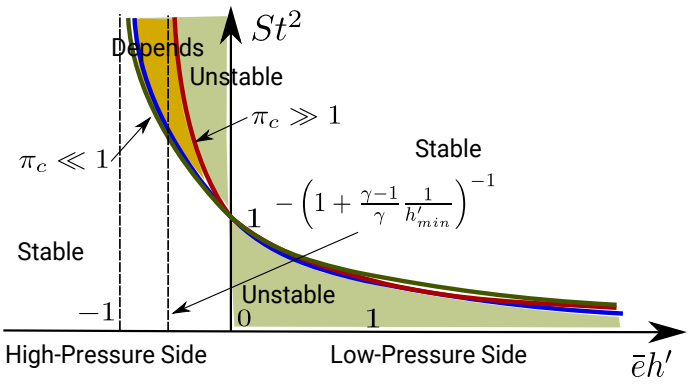

FIGURE 8. SCHEME OF THE SEAL STABILITY REGIONS OF A STRAIGHT SEAL AS A FUNCTION OF THE DIMENSIONLESS TORSION CENTER LOCATION. COMPARISON WITH THE ORIGINAL CV MODEL (BLUE CURVE).

ing in Eq. 29 that $\tilde{W}_{cyc}(St_c) = 0$. It is readily obtain that this condition yields:

$$St_c^2 = \frac{1}{1 + \tilde{e}h'_{eff}(\Omega, h')} \tag{36}$$

which is a generalization of the expression derived in [1]. The main difference with respect the isentropic model is that in this case Eq. 36 is an implicit definition of St_c. On the contrary than in the CV model, where $\tilde{e}h'$ was mainly a geometric parameter modulated by the pressure ratio, here $\tilde{e}h'_{eff}$ is a function of $\Omega = \Omega(St)$. The vibration angular frequency, ω, appears both in Ω and St, and therefore St_c cannot be explicitly derived. The linear relationship between Ω and St is actually:

$$\frac{\Omega}{St} = \frac{ND}{R}\frac{p_{c,s}V_{c,s}}{\dot{m}_s a_0} \tag{37}$$

which depends on the base flow, the seal geometry and the ND.

Despite this formal difficulty, it is possible to understand the new stability criterion as a perturbation of the CV stability criterion. Figure 8 sketches the extended CV region taking into account the dependencies of $\tilde{e}h'_{eff}$. The new criterion follows approximately the previously derived criterion (the blue line) especially for seal supported in the LPS ($\tilde{e}h' > 0$). For each frequency there is an upper and a lower bound whose amplitude depends on the frequency and the pressure ratio. The two limiting curves are obtained for a seal with a very low-pressure ratio (green curve) and for a choked seal (red curve).The largest differences between the current and the isentropic model are found for the HPS, whereas the stability limit for the LPS remains nearly unaltered.

The limiting value of $\tilde{e}h'$ below which seals supported in the HPS are always stable oscillates between $\tilde{e}h' = -1$ for very low pressure ratios ($h' \to \infty$) and $\tilde{e}h' \simeq -0.89$ for choked seals ($h' = 2.5$) (see Fig. 8). The stability of the seals whose torsion centers are located in this region is very sensitive to the pressure ratio.

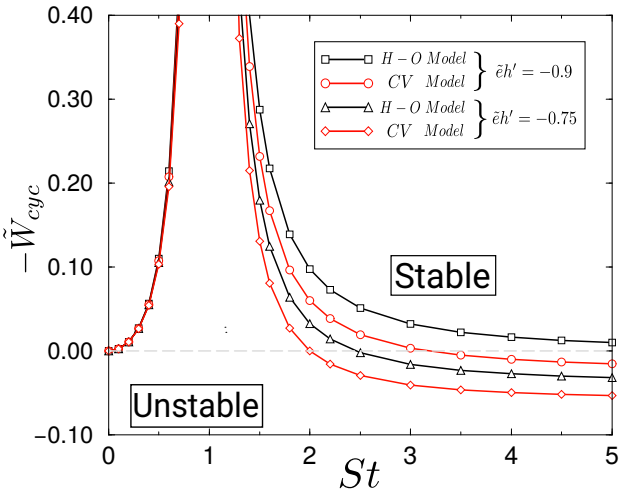

FIGURE 9. COMPARISON BETWEEN THE H-O MODEL (BLACK LINES) AND THE CV MODEL (RED LINES) FOR TORSION CENTERS LOCATED IN THE HIGH-PRESSURE SIDE. DIMENSIONLESS WORK-PER-CYCLE AS A FUNCTION OF THE RATIO BETWEEN THE VIBRATION FREQUENCY AND THE ACOUSTIC FREQUENCY, St. ($\Omega = 10$, $h' = 2.5$)

Figure 9 compares the work-per-cycle of the high-order model with that of the isentropic model for a two-fin choked seal with the torsion centers located in the aforemetioned critical region of the HPS. The largest differences are expected for this case. The curves are obtained by keeping the pressure ratio ($h' = 2.5$) and the non-dimensional frequency ($\Omega = 10$) constant. As expected, for $\tilde{e}h' = -0.9$ the original CV model predicts that the seal is stable up to a certain value of the reduced frequency ($St \simeq 3$), after which it becomes unstable. On the contrary, the higher order model is stable independently of St. In fact for a choked seal the limiting value of $\tilde{e}h'$ on the HPS below which the seal is always stable, is around -0.89. The difference on the critical reduced frequency predicted by the two models decreases with $\tilde{e}h'$. For $\tilde{e}h' = -0.75$ the new model predicts a critical reduced frequency of $St_c \simeq 2.5$, whereas the original CV model predicts $St_c \simeq 2$. Both models predict nearly the same St_c when $St < 1$. It is concluded that the critical frequency of the seal is sensitive to the model details when the torsion center is located on the HPS.

Taking into account the new non-dimensional parameter, $\tilde{e}h'_{eff}$, it can be concluded that the non-dimensional work-per-cycle of a two-fin stepped seal depends on four dimensionless parameters:

$$\tilde{W}_{cyc} = \tilde{W}_{cyc}\left(\tilde{\Omega}, St, \tilde{e}h'_{eff}, h'\right). \tag{38}$$

As it has been mentioned before the dependence of the $\tilde{W}_{cyc}$ on h' is a new finding and caused by the new barotropic relationship which is a function of the frequency.

The functional form of the new model is very similar to the original CV model [1] once the complexity has been abstracted using

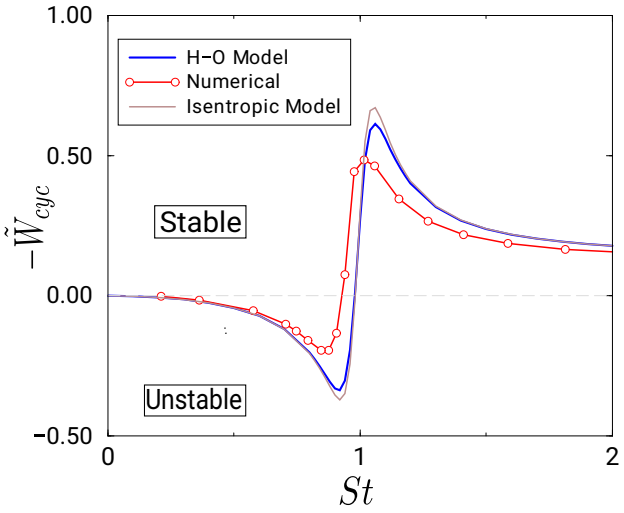

(a) Low-pressure side

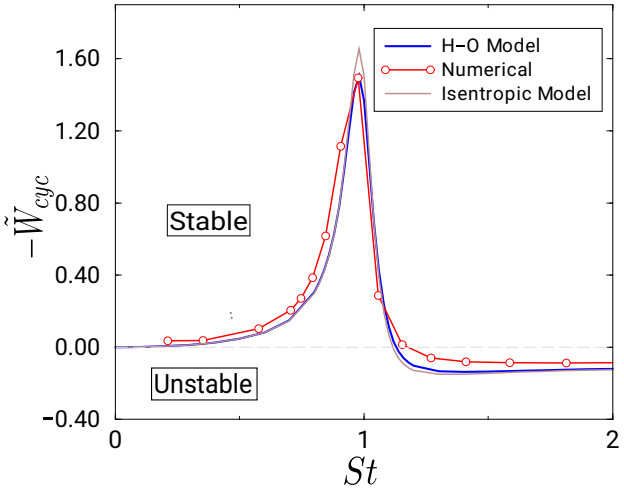

(b) High-pressure side

FIGURE 10. DIMENSIONLESS WORK-PER-CYCLE AS A FUNCTION OF THE RATIO BETWEEN THE VIBRATION FREQUENCY AND THE ACOUSTIC FREQUENCY, St. COMPARISON BETWEEN- THE MODEL AND LINEARIZED NAVIER-STOKES SIMULATIONS OF A TWO-FIN STRAIGHT SEAL WITH A PRESSURE RATIO OF 2.0 ($h' = 2.87$ AND $\bar{\Omega} = 7.6$) FOR A TYPICAL CASE IN THE LPS: $r/L = 0.5$, $\tilde{e}h' = 0.04$, (A) AND IN THE HPS: $r/L = -4$, $\tilde{e}h' = -0.2$, (B) .

proper variables such as $\bar{\Omega}$ and $\tilde{e}h'_{eff}$. Therefore, the structure of the solution will not be discussed here.

Preliminary CFD exploration Figure 10 compares the $\tilde{W}_{cyc}$ obtained from the model and data extracted from a frequency domain linearized Navier-Stokes solver for two different positions of the torsion center. The shape of the $\tilde{W}_{cyc}$ curves as a function of St is discussed in [1] and can be summarized as follows. The resonant condition is always stable, and for high vibration frequencies is achieved at $St \simeq 1$. That condition corresponds to the maximum of the $\tilde{W}_{cyc}$ (Eq. 29) which is proportional to $\bar{\Omega}\tilde{e}h'_{eff}$. The minimum of the function shown in Eq. 29 is always unstable and proportional to $\frac{1}{4\bar{\Omega}\tilde{e}h'_{eff}}$, except for $\tilde{e}h' < -1$ where the seal is stable independently of St. The matching is very good considering that an analytical expression results are compared with the CFD results. However, as highlighted before, special care must be taken to provide the proper data to the model that is extracted from the steady CFD analysis. The methodology employed here has been briefly described in the previous section. As mentioned before, the discussion about the numerical details of the simulations is postponed to a future paper since there are a large number of considerations to be taken into account. Nevertheless the qualitative and quantitative matching of both curves is excellent.

It is important to highlight that the simulations included in Fig. 10 are performed for a constant frequency by varying St changing the ND. This strategy was followed in order to control the acoustic resonances of the cavities located upstream and downstream of the seal. Since the frequency is high and $\Omega \gg 1 (\Omega = 22)$ the difference between the two analytical models reduces to a small difference in the resonance. In this particular case, the shift in the stability limit is very small since $\tilde{e}h' = 0.04$, is very small. Ten per cent variation in $\tilde{e}h'$ does not make any difference in practice.

The work presented here shows that the results analytically derived from first principles compare very well with the CFD results. This goes beyond a stability criterion since the model is able to provide the work-per-cycle in a variety of situations.

CONCLUDING REMARKS

An existing conceptual analytical model to assess the aeromechanics stability trends of labyrinth seals has been extended to account for non-isentropic flow perturbations. It is shown that the new model is qualitatively identical to the previously published model [1], especially in the range of industrial interest where the vibration frequency of the seal is high. The largest differences are seen for seal supported on the HPS at relatively low frequencies whose characteristic time is of the same order as that of the discharge time of the seal. This regime is of modest engineering interest since it is usually far way from the acoustic frequency of the seal cavity. For torsion centres located on the HPS and vibration frequencies comparable to the acoustic frequency, a difference of approximately 10% in the limiting position of the torsion centre with respect the original CV model can be seen.

A selected but reduced set of simulations has been included to assess the trends and accuracy of the model which ultimately reduce to a simple analytical expression. It is concluded that the

main difficulty in comparing CFD data and model is to inform the latter with the correct parameters derived from the steady numerical simulations, especially the effective gaps. The geometrical closures are of little help and discharge coefficients derived from steady CFD analysis need to be injected in the model. All the trends of the work-per-cycle derived from the CFD model are included in the model.

The new model is as simple to apply as the original one though the expressions are more involved. However, the model can be built in the same way as the original one. The credibility of the model to predict the stability trends is high since there is no known stability trend which had not been predicted up to now. In this work, the evidences supporting the model are increased by including a few selected CFD analysis. A large set of CFD cases exploring the model is in place but it has not been possible to include it here because of space and time limitations.

ACKNOWLEDGMENTS

Roque Corral wish to thank ITP Aero for allowing the publication of this paper and for its support during the project. Michele Greco wants to thank ITP by providing access to ITP's computing framework and its support. This research work was partially supported by the European project ARIAS, H2020 research and innovation program under grant agreement No. 769346. The authors gratefully acknowledge the financial support.

NOMENCLATURE

a_0	Sound speed in the cavity
A	Seal clearance area
a	Seal clearance area variation
d	Unit distance in the circumferential direction
$\tilde{e}$	$= \gamma r H/(sL)$ Non-dimensional torsion centre or seal clearance
h'	Non-dimensional seal pressure ratio parameter
E	$= C_v T + \frac{1}{2}\mathbf{v}^2$. Total internal energy
Ec	Eckert number
H	Fin clearance. Also total enthalpy $H = C_p T + \frac{1}{2}\mathbf{v}^2$.
HPS	High Pressure Side
L_θ	$= R/ND$, Circumferential wave length
L	Seal cavity length
LPS	Low- Pressure Side
CFD	Computational Fluid Dynamics
$\dot{m}$	Mass flow per span-wise or circumferential length unit
ND	Nodal diameter
ODE	Ordinary Differential Equation
PDE	Partial Differential Equation
p_c	Cavity static pressure
p_e	Exit static pressure
P_0	Inlet total pressure
Pr	Prandtl number
r	Torsion center position
R	Cavity radius
Re	Reynolds number
s	Cavity height
S	$= 2\pi RL$ Seal surface
St	Vibration-to-acoustic frequency ratio
TC	Torsion center
TW	Traveling-Wave Coordinate
t_d	$= \frac{p_{c,s} V_{c,s}}{\dot{m}_s a_0^2}$. Seal discharge time
t_p	Propagation time of circumferential waves
v_θ	Circumferential velocity
v	Volume variation
W_{cyc}	Work per cycle
z	Azimuthal coordinate

Greek symbols

α	Auxiliary function
δ	$= r\Delta\theta$ Seal displacement
γ	Heat capacity ratio
$\Delta\theta$	Rotation angle
η	$= \tau + \tilde{z}$. Non-dimensional TW coordinate
π	$= P_0/p_c$. Cavity pressure ratio
π_T	$= P_0/p_e$. Total pressure ratio
π_c	$= \pi_T/\pi$. Pressure ratios relationship
ρ	Fluid density
τ	Non-dimensional time
ω	Vibration angular frequency (rad/s)
Ω	$=\omega t_d$ Non-dimensional discharge time
$\tilde{\Omega}$	$=\Omega/h'$ Convenient form for Ω in the isentropic model
$\bar{\Omega}$	Convenient function to relate the new and the CV model

Super-scripts

˜	Non-dimensional values
ˆ	Normalized values
’	Time perturbation

Sub-scripts

e	Exit
c	Cavity
eff	Effective value
cyc	Per-cycle
s	Steady state
2D	per-unitary span of the inter-fin cavity

References

[1] Corral, R., and Vega, A., 2018. "Conceptual flutter analysis of labyrinth seals using analytical models. part i: Theoreti-

cal background". *ASME J. Turbomach.,* **140**(10), October, p. 121006.
[2] Chupp, R., Hendricks, R., Lattime, S., and Steinetz, B., 2006. "Sealing in turbomachinery". *AIAA Journal of Propulsion and Power,* **22**(2), March, pp. 314–349.
[3] Vahdati, M., Smith, N., and Zhao, F., 2015. "Influence of intake on fan blade flutter". *ASME J. Turbomach,* **137**(8), Aug, p. 081002.
[4] Corral, R., and Vega, A., 2016. "The low reduced frequency limit of vibrating airfoils - part i: Theoretical analysis". *ASME J. Turbomach,* **138**(2), February, p. 021004.
[5] Corral, R., Beloki, J., Calza, P., and Elliot, R., 2019. "Flutter generation and control using mistuning in a turbine rotating rig". *AIAA Journal,* **57**(2), February, pp. 782–795.
[6] Stapelfeldt, S., and Vahdati, M., 2019. "Improving the flutter margin of an unstable fan blade". *ASME J. Turbomach,* **141**(7), July, p. 071006.
[7] Alford, J. S., 1971. "Labyrinth seal designs have benefitted from development and service experience". In SAE Technical Paper, SAE International.
[8] Alford, J. S., 1975. "Nature, causes and prevention of labyrinth air seal failures". *AIAA Journal of Aircraft,* **12**(4), April, pp. 313–318.
[9] Lewis, D., Platt, C., and Smith, E., 1979. "Aeroelastic instability in f100 labyrinth air seals". *AIAA Journal of Aircraft,* **16**(7), pp. 484–490.
[10] Vega, A., and Corral, R., 2018. "Conceptual flutter analysis of labyrinth seals using analytical models. part ii: Physical interpretation". *ASME J. Turbomach.,* **140**(10), October, p. 121007.
[11] Corral., R., Greco, M., and Vega, A., 2019. "Tip-shroud labyrinth seal impact on the flutter stability of turbine rotor blades". *ASME J. of Turbomachinery,* **141**(10), October, p. 101006.
[12] Corral., R., Vega, A., and Greco, M., 2020. "Conceptual flutter analysis of stepped seals". *ASME J. Eng. Gas Turbines Power,* **142**(7), July, pp. 071001–1–9.
[13] Miura, T., and Sakai, N., 2019. "Numerical and experimental studies of labyrinth seal aeroelstic instability". *ASME J. Eng. Gas Turbines Power,* **141**(11), November, p. 111005.
[14] Alford, J., 1964. "Protection of labyrinth seals from flexural vibration". *ASME J. Eng. Gas Turbines Power,* **86**(2), October, pp. 141–147.
[15] Alford, J., 1967. "Protecting turbomachinery from unstable and oscillatory flows". *ASME J. Eng. Gas Turbines Power,* **89**, pp. 513–528.
[16] Ehrich, F., 1968. "Aeroelastic instability in labyrinth seals". *ASME J. Eng. Gas Turbines Power,* **90**(4), October, pp. 369–374.
[17] Abbot, D. R., 1981. "Advances in labyrinth seal aeroelastic instability prediction and prevention". *ASME J. Eng. Gas Turbines Power,* **103**(2), April, pp. 308–312.
[18] Zhuang, Q., 2012. "Parametric study on the aeroelastic stability of rotor seals". Master's thesis, Royal Institute of Technology.
[19] Hirano, T., Guo, Z., and Kirk, R. G., 2005. "Application of computational fluid dynamics analysis for rotating machinery-part ii: Labyrinth seal analysis". *ASME J. Eng. Gas Turbines Power,* **127**(4), September, pp. 820–826.
[20] Mare, L. D., Imregun, M., Green, J., and Sayma, A. I., 2010. "A numerical study on labyrinth seal flutter". *ASME J Tribology,* **132**(2), pp. 022201–7.
[21] Corral, R., and Vega, A., 2016. "Physics of vibrating turbine airfoils at low reduced frequency". *AIAA Journal of Propulsion and Power,* **32**(2), March, pp. 325–336.
[22] Corral, R., and Vega, A., 2017. "Quantification of the influence of unsteady aerodynamic loading on the damping characteristics of oscillating airfoils at low reduced frequency. part i: Theoretical support". *ASME J. Turbomach,* **139**(3), December, p. 0310009.
[23] Vega, A., and Corral, R., 2016. "The low reduced frequency limit of vibrating airfoils - part ii: Numerical experiments". *ASME J. Turbomach,* **128**(2), February, p. 021005.
[24] Vega, A., and Corral, R., 2017. "Quantification of the influence of unsteady aerodynamic loading on the damping characteristics of oscillating airfoils at low reduced frequency. part ii: Numerical verification". *ASME J. Turbomach,* **139**(3), June, p. 031010.
[25] Corral, R., Escribano, A., Gisbert, F., Serrano, A., and Vasco, C., 2003. "Validation of a linear multigrid accelerated unstructured navier-stokes solver for the computation of turbine blades on hybrid grids". In AIAA Paper 2003-3326, 9th AIAA/CEAS Aeroacoustics Conference.
[26] Burgos, M., Chia, J., R.Corral, and C.Lopez, 2009. "Rapid meshing of turbomachinery rows using semi-unstructured multi-block conformal grids". *Engineering with Computers,* **26**(4), December, pp. 351–363.

A Charge and Discharge of Tanks

All the variants of the CV model are based on the assumption that there is a plenum, namely the inter-fin cavity, with an inlet located in the LPS fin and an exit in the HPS fin. One of the assumptions is that the seal gaps are small slots compared to the volume of the seal, i.e. $H_{1,2} \ll (sL)^{1/2}$. Essentially the model handles three equations, the integral form of the mass conservation in the inter-fin cavity, which is an ODE, the momentum equation in the azimuthal direction, a PDE, and the entropy conservation of the perturbed flow, which is and algebraic equation.

The hypothesis that the flow perturbations are isentropic is convenient because of its simplicity but was not properly justified in the derivation of the CV model [1]. Actually, Ehrich in his

pioneering article [16] assumed that the flow was iso-thermal. It will be shown that none of these hypotheses is fully correct.

In this appendix, the fundamentals of the physical principles for the derivation of a more complex seal model are established. In order to do that, we analyze here the much simpler case of the charge and discharge of a tank with a single exit or inlet as a prelude to the more complex case in which simultaneously coexist an inlet and an exit. The underlying problem of the CV model is that the hypothesis that the flow is isentropic is just a replacement for the energy equation that not always is true. Here, a more thorough analysis of this conceptual toy problem is performed.

The mass and energy conservation equations for a tank can be written as:

$$\begin{aligned} \frac{d(\rho_c V)}{dt} &= \mp \dot{m} \\ \frac{d(p_c V)}{dt} &= \mp(\gamma-1)\dot{m}H^* \end{aligned} \tag{A.1}$$

where $\dot{m}$ and $H_0$are the mass-flow and the total enthalpy, respectively, leaving or entering the tank. It is important to notice that the kinetic energy in the tank has been neglected and the energy stored in the tank becomes $\rho_c E_c V = (p_c V)/(\gamma-1)$. During a discharge process H^* is the enthalpy of the reservoir and $H^* = H_d$, whereas during a charge process $H^* = H_\infty$, where H_∞ is the ambient total enthalpy. For the sake of simplicity, we will assume that the volume of the tank is constant, though the analysis could be carried out without recurring to this simplification.

Discharge case. During a discharge process if we realize that

$$H_c = \frac{\gamma}{\gamma-1}\frac{p_c}{\rho_c}, \tag{A.2}$$

and injecting this expression and the mass conservation equation in the energy equation this becomes:

$$\frac{d}{dt}\left(\frac{p_c}{\rho_c^\gamma}\right) = 0 \tag{A.3}$$

which clearly indicates that the discharge process is isentropic. The physical meaning is that the flow leaves smoothly the domain if the exit nozzle is properly designed and the discharge process is actually isentropic.

Charge case. During the charge process the situation is somewhat different. The energy equation can be written as:

$$\frac{d(p_c V)}{dt} = (\gamma-1)\dot{m}H_\infty \tag{A.4}$$

which combined with the mass conservation equation becomes:

$$\frac{d(p_c V)}{dt} = (\gamma-1)H_\infty \frac{d(\rho_c V)}{dt} \tag{A.5}$$

Therefore, if the volume of the tank, V, is constant then

$$(p_c - (\gamma-1)H_\infty \rho_c) = \text{constant} \tag{A.6}$$

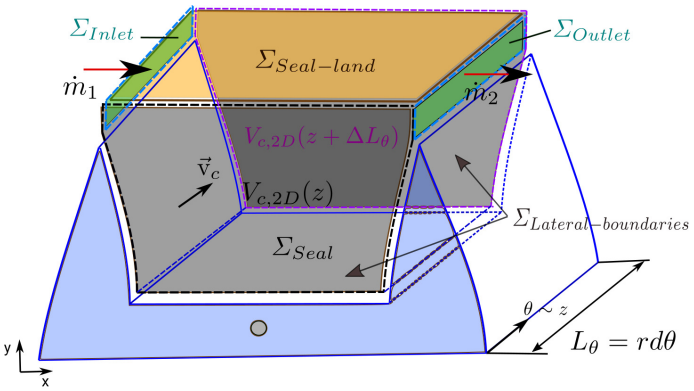

FIGURE B.1. CONTROL VOLUME AND NOMENCLATURE OF A INTER-FIN SEAL CAVITY.

It is obvious that during the charge process a barotropic relationship exists, i.e. $p = p(\rho)$, this is not neither the isentropic relationship, i.e. $p/\rho^\gamma =$ constant, nor the iso-thermal one, i.e. $p/\rho =$ constant. However, if the flow perturbations are small, Eq. A.6 implies that the flow perturbations are iso-thermal which was the hypothesis used by Ehrich [16]. The underlying physical reason of this result is that during the charge process, a jet is created and dissipated in the tank and therefore, the process is not isentropic anymore.

The conclusion from this appendix is that in a labyrinth seal, to use the hypothesis of either isentropic or isothermal flow for the perturbations is risky, since both inlet and outlets are present simultaneously and the integral equation of the energy should be used instead.

B Derivation of Semi-Integral Mass and Energy Equations

The objective of this appendix is to formally derive the semi-integral mass and energy equations for the inter-fin cavity. The mass conservation equation was informally derived in [1] but here we aim at a formal derivation of the semi-integral mass and energy equations. Figure B.1 sketches the control volume of the inter-fin cavity of the rotating seal and the nomenclature used in this appendix.

Continuity Equation

The integral form of the mass-conservation equation in an arbitrary control volume can be written as:

$$\frac{\partial}{\partial t}\int_\Omega \rho d\Omega + \int_{\Sigma_c} \rho(\mathbf{v}-\mathbf{v}_c).\mathbf{n}dA = 0 \tag{B.1}$$

where $\mathbf{v}$ is the fluid velocity, $\mathbf{v}_c$ the velocity of the control volume surface, and $\mathbf{n}$ the normal to the control volume surface pointing outwards. Defining the average density within the inter-fin cavity as:

$$\int_{\Omega} \rho d\Omega = \rho_c V_{c,2D} L_\theta \tag{B.2}$$

The control volume surface, Σ_c, can be decomposed into the sum of all its individual surfaces as:

$$\Sigma_c = \Sigma_{Inlet} + \Sigma_{Oulet} + \Sigma_{seal-land} + \Sigma_{Seal} + \Sigma_{Lateral-Boundaries} \tag{B.3}$$

The mass-flows through the seal land and the seal itself are zero. The latter because $\mathbf{v} = \mathbf{v}_c$ and the former because $\mathbf{v} = \mathbf{v}_c = 0$. The mass-flow per span unit through the inlet and the outlet are named $\dot{m}_1$ and $\dot{m}_2$ respectively. Equation B.1 then reduces to:

$$\frac{\partial \left(\rho_c V_{c,2D}\right)}{\partial t} + (\dot{m}_2 - \dot{m}_1) + \frac{\left(\rho_c v_\theta V_{c,2D}\right)_{z+\Delta L_\theta} - \left(\rho_c v_\theta V_{c,2D}\right)_z}{\Delta L_\theta} = 0 \tag{B.4}$$

where the last two terms correspond to the mass flux across the two azimuthal planes denoted in Fig. B.1 as lateral boundaries. In the continuous limit ($\Delta L_\theta \to 0$) Eq. B.4 becomes:

$$\frac{\partial}{\partial t}(\rho_c V_{c,2D}) + \dot{m}_2 - \dot{m}_1 + \frac{\partial}{\partial z}\left(\rho_c v_\theta V_{c,2D}\right) = 0 \tag{B.5}$$

which is exactly the same equation used throughout [1, 11, 12].

Energy Equation

The integral form of the mass-conservation equation in an arbitrary control volume neglecting viscous forces, body forces and the heat flux through the walls can be written as:

$$\frac{\partial}{\partial t}\int_{\Omega} \rho E \, d\Omega + \int_{\Sigma_c} \rho E \left(\mathbf{v} - \mathbf{v}_c\right).\mathbf{n} dA = -\int_{\Sigma_c} p \, \mathbf{v}.\mathbf{n} dA. \tag{B.6}$$

Analogously as in the continuity equation the mean average pressure within the inter-fin cavity can be defined as:

$$\int_{\Omega} \rho E \, d\Omega = \frac{1}{\gamma - 1} p_c V_{c,2D} L_\theta. \tag{B.7}$$

The internal energy flux, ρE, through the seal land seal and the seal itself are zero for the same reasons outlined in the mass-conservation equation. The right hand side of Eq.B.6 represents the work of the pressure on the surfaces of the control volume. Except in the land seal surface, $\Sigma_{land-seal}$, where the normal velocity is null, $\mathbf{v}.\mathbf{n} = 0$, in the rest of the surfaces this term cannot be neglected. In the non-moving surfaces, namely the inlet, the outlet, and the two lateral planes which close the domain, where $\mathbf{v}_c = 0$, this term can be combined with the total energy flux

$$\int_{\Sigma_c} \rho E \, \mathbf{v}.\mathbf{n} dA + \int_{\Sigma_c} p \, \mathbf{v}.\mathbf{n} dA = \int_{\Sigma_c} \rho H \, \mathbf{v}.\mathbf{n} dA \tag{B.8}$$

to yield the total enthalpy flux. The contribution of the pressure work in the moving seal where $\mathbf{v}.\mathbf{n} = \mathbf{v}_c.\mathbf{n} \neq 0$, can be expressed as:

$$\int_{\Sigma_c} p \, \mathbf{v}.\mathbf{n} dA = p_c \frac{\partial V_{c,2D}}{\partial t} \Delta L_\theta \tag{B.9}$$

which is nothing else than the mean cavity pressure multiplied by the variation of the volume of the inter-fin cavity. The energy equation of the inter-fin cavity can finally be written as:

$$\frac{1}{\gamma - 1}\frac{\partial}{\partial t}(p_c V_{c,2D}) + \dot{m}_2 H_2 - \dot{m}_1 H_1 + \frac{\partial}{\partial z}\left(\rho_c v_\theta H_c V_{c,2D}\right) = -p_c \frac{\partial V_{c,2D}}{\partial t} \tag{B.10}$$

where p_c, ρ_c and H_c represent the spatially averaged pressure, density and total enthalpy in the inter-fin cavity, respectively. Equations B.5 and B.10 are two PDEs referred to as the semi-integral form of the mass and energy equation since the circumferential variations are retained using spatial derivatives whereas the mass and energy flux through the inlet and the outlet are included in integral form.